Spectroscopy of the spatially-extended Lyα emission around a QSO at z=6.4

Tomotsugu Goto[1] , Yousuke Utsumi[2], Jeremy R. Walsh[3], Takashi Hattori[4],
Satoshi Miyazaki[2], and Chisato Yamauchi[5]

[1]*Institute for Astronomy, University of Hawaii 2680 Woodlawn Drive, Honolulu, HI, 96822, USA, tomo@ifa.hawaii.edu*
[2]*Department of Astronomical Science,The Graduate University for Advanced Studies, 2-21-1 Osawa, Mitaka, Tokyo 181-8588, Japan*
[3]*European Southern Observatory, Karl-Schwarzschild Strasse 2, D-85748, Garching, Germany*
[4]*Subaru Telescope 650 North A'ohoku Place Hilo, HI 96720, USA*
[5]*Institute of Space and Astronautical Science, Japan Aerospace Exploration Agency, Sagamihara, Kanagawa 252-5210*

ABSTRACT
We have taken a deep, moderate-resolution Keck/Deimos spectra of QSO, CFHQS2329, at
z=6.4. At the wavelength of Lyα, the spectrum shows a spatially-extended component, which
is significantly more extended than a stellar spectrum, and also a continuum part of the spec-
trum. The restframe line width of the extended component is 21±7 (Å), and thus smaller than
that of QSO (52±4Å) , where they should be identical if the light is incomplete subtraction
of the QSO component. Therefore, these comparisons argue for the detection of a spatially
extended Lyα nebulae around this QSO. This is the first z>6 QSO that an extended Lyα halo
has been observed around. Careful subtraction of the central QSO spectrum reveals a lower
limit to the $Lyα$ luminosity of $(1.7\pm0.1)\times10^{43}$ erg s^{-1}. This emission may be from the the-
oretically predicted infalling gas in the process of forming a primordial galaxy that is ionized
by a central QSO. On the other hand, if it is photoionized by the host galaxy, an estimated
star-formation rate of $>3.0\ M_\odot$ yr^{-1} is required.

If we assume the gas is virialized, we obtain dynamical mass estimate of M_{dyn}=1.2
$\times10^{12}M_\odot$. The derived M_{BH}/M_{host} is 2.1 $\times10^{-4}$, which is two orders smaller than those
from more massive z∼6 QSOs, and places this galaxy in accordance with the *local* M-σ re-
lation, in contrast to a previous claim on the evolution of M-σ relation at z∼6. We do not
claim evolution or non-evolution of the M-σ relation based on a single object, but our result
highlights the importance of investigating fainter QSOs at z∼6.

Key words: quasars:individual, black hole physics, galaxies: high-redshift

1 INTRODUCTION

Understanding the first stage of the formation of galaxies is one
of the central issues in observational astronomy. Galaxy formation
models predict that an early stage inevitably involves a spatially ex-
tended distribution of infalling, cold gas (Haiman & Rees 2001). If
such gas is ionized by a central luminous quasar (QSO), or an initial
starburst, such gas should be observed as extended Lyα emission
in the high-z Universe.

However, due to instrumental limitations, extensive searches
for extended Lyα emission or Lyα blobs were mostly conducted
at at z∼2-3 in the past (Steidel et al. 2000; Matsuda et al. 2004;
Nilsson et al. 2006; Smith & Jarvis 2007; Smith et al. 2009), with
only a few exceptions at z=6.595 (Ouchi et al. 2009) and at z=4.5
(Bunker et al. 2003). It is worth noting that some of these de-
tections are associated with a bright QSO (Bunker et al. 2003;
Weidinger et al. 2005; Barrio et al. 2008). If a QSO is a heating
source, it is also a subject of interest to understand what role a cen-

tral black hole plays in such an early stage of the galaxy formation,
perhaps leading to the tight correlations observed at low redshift
such as the M-σ relation (Magorrian et al. 1998), and the starburst-
AGN connection (Maiolino et al. 1997; Goto 2005, 2006).

However, at z=3, the age of the Universe was already 2.2 Gyrs,
and thus, it may be too late to search for a primordial stage of a
galaxy formation (Scannapieco et al. 2003). In Goto et al. (2009),
we found a spatially-extended structure around a QSO at z=6.4.
This may be the first example of $Lyα$ blob around a luminous
QSO at z>6. However, the detection was in the z'-band image
of Subaru/Suprime-Cam. Therefore, it was not clear if the ex-
tended structure was Lyα emission, or continuum emission from
the QSO host galaxy. In this work, we performed a deep, moderate-
resolution spectroscopy with the Keck/Deimos to clearly separate
the two cases. Unless otherwise stated, we adopt the WMAP cos-
mology: $(h, \Omega_m, \Omega_L) = (0.7, 0.3, 0.7)$.

Table 1. Target information adopted from Willott et al. (2007) and Goto et al. (2009).

Object	z_{MgII}	i'_{AB}	z'_{AB}	z_R	J
CFHQS J232908.28-030158.8	6.417±0.002	25.54±0.02	21.165±0.003	21.683±0.007	21.56±0.25
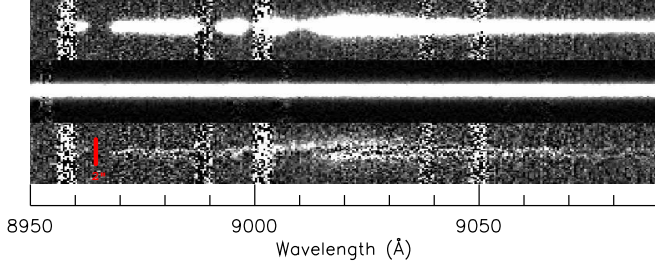
Figure 1. Subtracting stellar spectrum from QSO spectrum. The top panel shows the QSO spectrum. The middle panel is a reference PSF stellar spectrum. The bottom panel shows the residuals from the subtraction of the PSF spectrum and the smooth extended component from the QSO spectrum. Pixel scale in spatial direction is 0.1185" pix^{-1}. The red bar shows a scale of 2".

2 OBSERVATION

Our target is QSO CFHQS J2329-0301(Table 1; Willott et al. 2007) at z=6.417 (Willott et al. 2010). This QSO is known to be in a dense environment surrounded by 7 LBG candidates(Utsumi et al. 2010).

We obtained moderate resolution spectra of the QSO using Keck/Deimos on the nights of September 12 and 13, in 2010. The details of the observation and data reduction are described in Goto et al. (2011). Briefly, we used the 830 lines mm^{-1} grating and the OG550 order cut filter with the central wavelength of 8500Å . The slit width was 1.0" with 0.47 Å pixel^{-1}, giving a resolving power of $R \sim$3600. The position angle of the slit was -30 deg. The wavelength coverage was 6000Å to 10000Å. The spatial resolution is 0.1185" pixel^{-1}. The total integration time was 5.5 hours.

We used the Deep2 pipeline to reduce the data, except the background subtraction, which we did manually to remove ghost features of the 830 grating carefully. Wavelength calibration is based on the HeNeAr lamp.

For flux calibration, the spectrophotometric standard G191-B2B was observed and used to correct the spectral shape. Absolute flux calibration was achieved by passing the spectra of the QSO through the Subaru z' filter and normalizing to match the observed z' magnitude in Table 1. We independently performed the absolute flux calibration using the standard G191-B2B, obtaining only 4% larger absolute flux.

3 ANALYSIS

3.1 Removal of the QSO PSF

To investigate the extended component of the spectrum, we need to subtract the central point source spectrum, which is often brighter by a factor of >10 for a QSO. We chose a spectrum of a bright star in the same Deimos mask as the QSO and which was relatively free of the ghost features of the 830G grism; this spectrum is shown in the middle panel of Fig.1. The PSF of the QSO and the extended background were decomposed (in the spatial direction)

Table 2. Properties of Lyα emission from the extended region.

FWHM (Å)	Flux (erg cm^{-2} s^{-1})	Luminosity (erg s^{-1})	Velocity Disp. (km s^{-1})
21±7	(3.6±0.2) $\times 10^{-17}$	(1.7±0.1)$\times 10^{43}$	301±99

using the IRAF code *specinholucy* based on a two-channel restoration technique (Lucy & Walsh 2003). The technique restores the spatial profile of the PSF and a smooth background wavelength-by-wavelength. It is based on a two-channel restoration algorithm that restores a point spread function (PSF)-like component in a 2D spectrum and an underlying extended background component. It has already been successfully used to subtract point-source spectra in highly inhomogeneous backgrounds, such as high-z SNe Ia embedded in their host galaxy (Blondin et al. 2005). Therefore, it is also suitable for our case of separating QSO from the extended structure.

The top panel of Fig.1 shows the reduced 2D spectrum of J2329. The middle panel shows the spectrum of the reference PSF star. The PSF size (FWHM) measured from a star in a slit is 0.65".

The restored background component was smoothed by a Gaussian (see Lucy & Walsh 2003, for details) of FWHM 16.5 pixels (1.95"). On subtracting this smooth component from the spectrum (with the QSO PSF removed), structure at spatial scales intermediate between that of the PSF and the smooth extended structure was revealed. The bottom panel of Fig.1 shows this revealed component.

In the bottom panel of Fig.1, at the peak of the QSO spectrum, there remain positive and negative residuals resulting from incomplete PSF removal. This has often been seen in PSF removal and usually arises when the spatial profile of the PSF star does not quite match that of the target. The residuals are at the level of a few percent of the peak of the QSO PSF.

Noteworthy in Fig.1 is the extended flux over the wavelength range 9006-9035Å that remains from the decomposition. The peak of this flux corresponds to Lyα wavelength at the redshift of the QSO. The red bar of length 2" in the figure shows the spatial scale for reference, indicating that the remaining flux is spatially extended over an extent as large as $\sim$4". In Fig.2, we show the residual extended flux from the two-channel restoration summed in the wavelength direction over the extent 9006 to 9035Å. The error bars include Poisson noise from the QSO and star spectra, and the background noise. Compared with the errorbars, remaining flux from -1.7 to +1.6 arcsec appears to be significant.

To further verify this finding, in Fig.3, we compare the spatial flux profile in the wavelength range between 9006 and 9035Å of the QSO spectrum (corresponding to Lyα emission) in the black solid line, and that between 9058 and 9087Å(i.e., remote from the Lyα line) in the red dotted line. Both of these wavelength ranges are chosen so that they do not include strong sky emission lines. The flux profile of the star in the range of 9006-9035Å is also plotted in the blue dotted line. Compared with the associated errorbars, the flux profile of the QSO at the Lyα wavelength is significantly
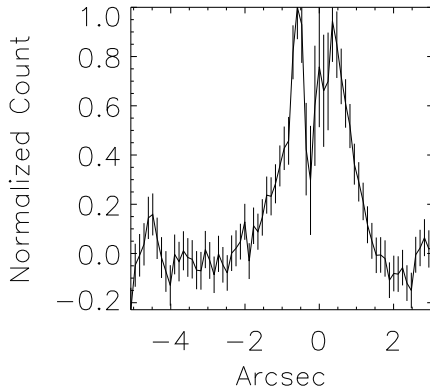
Figure 2. The residuals on the two channel restoration of the QSO 2D spectrum are shown summed in wavelength from 9006 to 9035Å. The error bars include those of the QSO, the star, and the background noise.
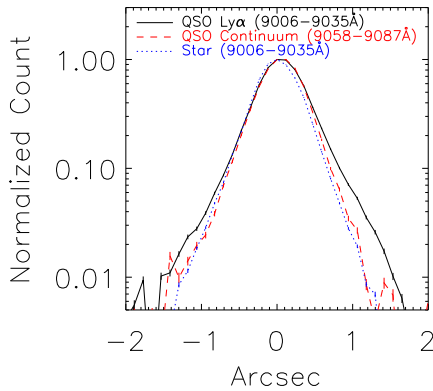
Figure 4. One-dimensional spectra of the extended region of CFHQSJ2329 after subtracting the central QSO. The gray line shows spectrum in the original resolution. The black line shows binned spectrum with 10 pixel box. The magenta dash-dotted lines show the sky spectrum in an arbitrary unit. The blue dotted line shows the arbitrary-scaled spectrum of the QSO.

3.2 One dimensional spectrum

On the basis of this evidence, we claim that at least the Lyα region of the spectrum is more extended than the PSF from the star and the continuum region of the QSO spectrum. Next, we extracted a one-dimensional spectrum from the 2D image by masking out the central 10 pixels (1.1"), where the residuals on the PSF match are strong. Note that due to this masking, the computed flux and luminosity are lower limits.

In Fig.4, we show the one-dimensional spectrum. The gray line shows the spectrum at the original resolution. The black line shows the same spectrum binned with a 10 pixel box. The magenta line shows the scaled sky spectrum. As expected from Fig.1, a strong peak can be seen at around Lyα emission. Due to neutral hydrogen absorption on the bluer side, the line has clear asymmetric profile with an extended red wing that is typical for a high-z Lyα line. In the blue dotted line, we show the arbitrary-scaled QSO spectrum before the PSF subtraction. The Lyα line profile of the QSO is much broader. This difference confirms that the residual in the bottom panel of Fig.1 is not part of the (unsubtracted) QSO spectrum, but indeed spectrum of a different nature.

The total flux measured between 9006 and 9035Å region (except central 1") is $(3.6\pm0.2) \times10^{-17}$ erg cm$^{-2}s^{-1}$ as shown in Table 2. Compared with errors measured from 9058-9087Å region of the spectrum, this is a 17 σ detection. There is no significant flux detected other than the Lyα wavelength. The flux corresponds to the lower limit of Lyα luminosity of $(1.7\pm0.1)\times10^{43}$ erg s^{-1} (c.f., the Lyα luminosity of the QSO is 6.2×10^{44} erg s^{-1}). This is smaller than photometrically estimated value of 2.0×10^{43} erg s^{-11} (Goto et al. 2009), but consistent with each other, since our estimate is a lower limit due to the central mask. For comparison,

Figure 3. Comparison of the spatial profiles of the QSO spectrum over the Ly-α line between 9006 and 9035Å (black solid line), and over the continuum between 9058 and 9087Å (red dotted line). The blue dotted line show the spatial profile of a star between 9006 and 9035Å.

more extended than that of the continuum, and the star. We also performed a 2-dimensional subtraction using the QSO continuum as a spectral PSF, interpolating the PSF shape from the continuum on both sides of the Lyα line, obtaining a very similar result as in Fig.1. Note that the continuum region may contain an extended component from the underlying galaxy. This test was performed in case the optical distortions in the spectrograph differ between the position of the star used as a PSF and QSO slit position. However, the spatial profiles of the star and QSO continuum are very similar (see Fig. 3), suggesting such effects are small.

We note that the extended emission may be stronger above than below the QSO spectrum in Fig.1. Corresponding asymmetry can be found in Fig.2. This can also be seen in Fig.3, where the excess from the continuum subtraction is larger at the positive offset. Also the emission may be tilted in wavelength-position space as revealed in the bottom panel of Fig.1. This may be a sign of rotation in the extended Lyα emitting region, but needs confirmation from a better spatial resolution spectrum.
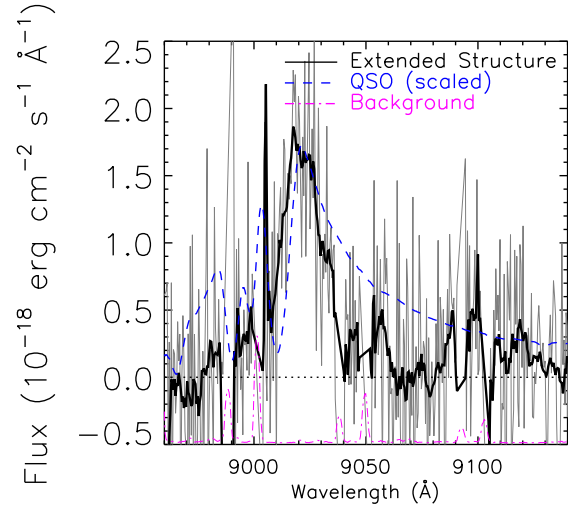
[1] Goto et al. (2009) had a computational error. We quoted a corrected value here.
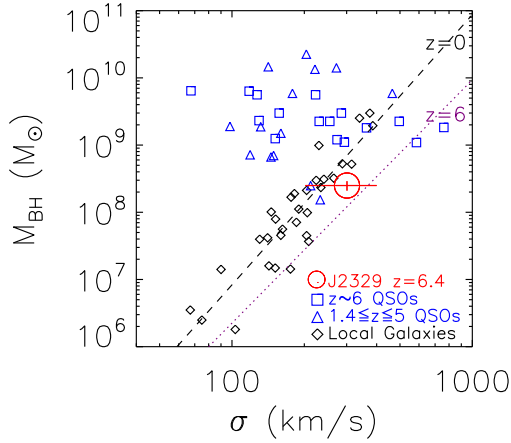
Figure 5. $M_{BH} - \sigma$ relation. The data points except for J2329 are adopted from Wang et al. (2010). The diamonds represent the local galaxies (Tremaine et al. 2002), whose local $M_{BH} - \sigma$ relationship in the black dashed line is $\log(M_{BH}/M_\odot) = 8.13 + 4.02\log(\sigma/200\,\mathrm{km\,s^{-1}})$. The blue squares and triangles are for the z~6 and $1.4 \leqslant z \leqslant 5$ QSO samples, respectively, with σ derived from the observed CO line width using $\sigma \approx FWHM/2.35$ (Wang et al. 2010). The red circle show J2329 at z=6.4 measured in this work based on the dispersion of the Lyα line. The purple dotted line shows a simulated M-σ relation at z=6 (Robertson et al. 2006).

the luminosity of a Lyα blob at $z \sim 6.5$ is $L^* \sim 3.9 \pm 0.2 \times 10^{43}$ erg s^{-1} (Ouchi et al. 2009) and Lyα blobs at z=3.1 is $\sim 1 \times 10^{43}$ erg s^{-1} (Matsuda et al. 2004, 2006).

The FWHM estimated through a Gaussian fit is 21 ± 7 (Å) in the restframe. This narrow width of the line also suggests that the Lyα emission did not originate from the broad line regions of the QSO (FWHM of 52 ± 4Å). We do not recognize the presence of a clear rotation curve, or multiple velocity components. In terms of velocity dispersion in the restframe, this corresponds to 301 ± 99 km s^{-1}. For comparison, the median velocity dispersion of Lyα blobs at z=6.6 is 110 km s^{-1} (Ouchi et al. 2009), and at z=3.1 is 330 km s^{-1} (Matsuda et al. 2004, 2006).

If the nebula forms a single virialized system with a velocity dispersion of 301 km s^{-1} in 2" radius (11 kpc at z=6.4), we estimate a virial mass of $1.2 \times 10^{12} M_\odot$ ($5/3 \times 3\sigma^2 R/G$). For comparison, Goto et al. (2009) estimated a stellar mass from 6.2×10^8 to $1.1 \times 10^{10} M_\odot$ depending on the star-formation history. If the velocity dispersion of the nebula reflects the dynamics of the host galaxy, it suggests that a massive galaxy is already harboring a QSO at z=6.4.

3.3   Non-detection of Continuum

Goto et al. (2009) detected 2.5×10^{-19} erg cm^{-2} s^{-1} Å^{-1} of flux density from the extended component in z_r filter (λ_e=988nm) at 3 σ. We did not detect any continuum from the extended component other than the Lyα emission. However, the noise level of our continuum is 5.5×10^{-19} erg cm^{-2} s^{-1} Å^{-1} pixel^{-1}. Therefore, we cannot indicate the detection or non-detection of the possible continuum emission from the extended component.

Since we did not detect continuum from the extended component, we cannot obtain an equivalent width (EW) solely from the spectra. However, if we use the continuum level of z_r band, we ob-

tain the restframe EW of 19 ± 6 Å. This is not a particularly large value for Lyα blobs. For example, all 18 Lyα blobs in Saito et al. (2008) had EW$_{rest} > 100$Å (but not all of them are associated with a QSO).

4   DISCUSSION

4.1   Comparison to Lyα blobs around low-z QSOs

It is informative to compare the size of the extended Ly-α emission around CFHQS J232908.28-030158.8 with that of similar structures, Ly-α blobs around lower redshift QSOs. Barrio et al. (2008)'s Lyα nebula around a z=2.48 QSO had FWHM$_{rest}$ of 370 ± 63 km/s, with 40 kpc radius of extension (in 3 separate parts though). The Lyα halo around a radio-quiet QSO at z=3.04 also extended to ~30 kpc (Weidinger et al. 2005). Bunker et al. (2003) reported a 5"-extended, FWHM$_{rest}$ of 181 km/s Lyα nebula around a QSO at z=4.5. Compared to these, our z=6.4 Lyα nebula has a much larger FWHM$_{rest}$ of 707 ± 232 km/s, perhaps reflecting a larger M_{host}. Although the 11 kpc of extension is smaller than the measured sizes at lower-z, surface brightness dimming is much greater at z=6.4, and thus, the size could be larger than measured. There exist only a few examples of extended Lyα halos around QSOs. It is important to construct a larger sample to correctly understand the evolution of the Lyα halo around QSOs.

4.2   What is the physical origin of this Lyα nebula?

Since there exists a QSO at the center of this nebula, an obvious explanation is halo gas photoionized by the QSO. Following Yu & Lu (2005), we estimate the ionizing photon emission rate of this QSO using absolute magnitude $M_{1450\mathring{A}}$=-25.23 (Willott et al. 2007). We count photons with energy in the range 13.6-54.4 eV as ionizing photons. We assumed average QSO SEDs at $z > 3$ from Telfer et al. (2002). To be conservative, we used the SED of radio-loud QSOs, which produce smaller ionizing photon rates than radio-quiet QSOs. The rate obtained for the QSO is $1.6 \times 10^{56} s^{-1}$. On the other hand, Ly$\alpha$ photon rate emitted by the nebula is several $10^{53} s^{-1}$. Therefore, there are orders more ionizing photons produced by the QSO to illuminate the Lyα nebula. A cold accretion of neutral gas (Barkana & Loeb 2003), or recently found re-scatted Lyα photons by neutral hydrogen (Hayes et al. 2011) are other candidates to explain Lyα blobs. In our case, however, these scenarios are unlikely because neutral hydrogen cannot survive exposure to the abundant ionizing photons.

In addition, star-formation in the host galaxy can also contribute (Taniguchi & Shioya 2000; Ohyama et al. 2003). The star-formation rate (SFR) can be estimated using the following relation (Kennicutt 1998; Taniguchi et al. 2007).

$$SFR(Ly\alpha) = 9.1 \times 10^{-43} L(Ly\alpha) M_\odot yr^{-1}, \qquad (1)$$

Based on the Lyα luminosity, we estimate the SFR(Lyα) is >3.0 $M_\odot$ yr^{-1}. This is not a high SFR, and thus, can be expected from a young star-forming galaxy. Therefore, it is possible that the star-formation in the host galaxy contributes to ionizing the Lyα nebula.

4.3 $M_{BH} - \sigma$ relation at $z > 6$

The virial mass estimate provides an interesting opportunity to investigate the M_{BH}/M_{host} ratio at z> 6. The black hole mass of this QSO was measured to be $2.5 \pm 0.4 \times 10^8 M_\odot$ based on the MgII

line and $L_{3000\overset{\circ}{A}}$ (Willott et al. 2010). Combined with our virial mass of $1.2 \times 10^{12} M_{\odot}$, we obtain M_{BH}/M_{host} of 2.1×10^{-4}. This value is much smaller than those previously measured from brighter QSOs at z∼6. For example, Wang et al. (2010) obtained a median M_{BH}/M_{bulge} ratio of 0.022 for bright ($M_{BH} > 10^9 M_{\odot}$) QSOs at z∼6, leading to a discussion that super massive BHs at z∼6 grow rapidly without commensurate growth of their host galaxies. On the contrary, this QSO is consistent with the local M-σ relation as shown in Fig.5.

Based on their galaxy merger simulations, Robertson et al. (2006) predicted a weak redshift-dependent shift in the M-σ relation due to an increasing velocity dispersion for a given galactic stellar mass. This QSO is even consistent with their predicted M-σ relation at z=6 shown in the purple dotted line in Fig.5. Note, however, that our measurement is made under the assumption that the gas is virialized. It is assumed that there is no effect on the measured line profile from non-kinematic broadening mechanisms (such as resonant atomic scattering or dust scattering).

We do not claim an evolution or non-evolution of the M_{BH}/M_{bulge} ratio based on one data point at z=6.4. However, due to the optical selection limit, previous QSO samples at z∼6 were limited to extremely massive BHs with $M_{BH} > 10^9 M_{\odot}$, sampling only a small range in BH mass. Combined with errors in measuring velocity dispersion, this may have been one of the reasons why an almost flat $M_{BH} - \sigma$ relation was found at z∼6 (Shields et al. 2006; Wang et al. 2010), and shown in Fig.5. Our result with a fainter QSO highlights the importance of sampling a wider range in M_{BH} to more accurately assess the $M_{BH} - \sigma$ relation at z∼6. Extended Lyα emission around a QSO may offer an alternative way to investigate fainter QSOs, whose molecular gas lines cannot be easily observed with existing facilities.

4.4 Note added at revision

After this paper was submitted and a referee's report received, an observational spectroscopic study of the identical QSO appeared on arXiv. Willott et al. (2011) observed the same Ly-α halo with Keck/ESI for 8.5 hours in seeing of 0.93" They found $L_{Ly\alpha} > 8 \times 10^{43}$ erg/s, with an extension of over 15 kpc, and a FWHM of 640 km/s. However, in contrast to the work presented here, an independent PSF was not available to remove the underlying QSO continuum. We show here that the results are very similar if a PSF star or the QSO continuum are utilised to remove the QSO across the Ly-α line, thus independently strengthening the result in Willott et al. In consequence the numbers for the extended Ly-α flux and width reported in Willott are consistent with the findings in this paper.

REFERENCES

Barkana R., Loeb A., 2003, *Nature* , 421, 341
Barrio F. E., Jarvis M. J., Rawlings S., et al., 2008, *MNRAS* , 389, 792
Blondin S., Walsh J. R., Leibundgut B., Sainton G., 2005, *AAp* , 431, 757
Bunker A., Smith J., Spinrad H., Stern D., Warren S., 2003, *ApSS* , 284, 357
Goto T., 2005, *MNRAS* , 360, 322
Goto T., 2006, *MNRAS* , 369, 1765

Goto T., Utsumi Y., Furusawa H., Miyazaki S., Komiyama Y., 2009, *MNRAS* , 400, 843
Goto T., Utsumi Y., Hattori T., Miyazaki S., Yamauchi C., 2011, *MNRAS* , 415, L1
Haiman Z., Rees M. J., 2001, *ApJ* , 556, 87
Hayes M., Scarlata C., Siana B., 2011, *Nature* , 476, 304
Kennicutt Jr. R. C., 1998, *ARAA* , 36, 189
Lucy L. B., Walsh J. R., 2003, *AJ* , 125, 2266
Magorrian J., Tremaine S., Richstone D., et al., 1998, *AJ* , 115, 2285
Maiolino R., Ruiz M., Rieke G. H., Papadopoulos P., 1997, *ApJ* , 485, 552
Matsuda Y., Yamada T., Hayashino T., et al., 2004, *AJ* , 128, 569
Matsuda Y., Yamada T., Hayashino T., Yamauchi R., Nakamura Y., 2006, *ApJL* , 640, L123
Nilsson K. K., Fynbo J. P. U., Møller P., Sommer-Larsen J., Ledoux C., 2006, *AAp* , 452, L23
Ohyama Y., Taniguchi Y., Kawabata K. S., et al., 2003, *ApJL* , 591, L9
Ouchi M., Ono Y., Egami E., et al., 2009, *ApJ* , 696, 1164
Robertson B., Hernquist L., Cox T. J., et al., 2006, *ApJ* , 641, 90
Saito T., Shimasaku K., Okamura S., et al., 2008, *ApJ* , 675, 1076
Scannapieco E., Schneider R., Ferrara A., 2003, *ApJ* , 589, 35
Shields G. A., Menezes K. L., Massart C. A., Vanden Bout P., 2006, *ApJ* , 641, 683
Smith D. J. B., Jarvis M. J., 2007, *MNRAS* , 378, L49
Smith D. J. B., Jarvis M. J., Simpson C., Martínez-Sansigre A., 2009, *MNRAS* , 393, 309
Steidel C. C., Adelberger K. L., Shapley A. E., Pettini M., Dickinson M., Giavalisco M., 2000, *ApJ* , 532, 170
Taniguchi Y., Ajiki M., Nagao T., et al., 2007, *PASJ* , 59, 277
Taniguchi Y., Shioya Y., 2000, *ApJL* , 532, L13
Telfer R. C., Zheng W., Kriss G. A., Davidsen A. F., 2002, *ApJ* , 565, 773
Tremaine S., Gebhardt K., Bender R., et al., 2002, *ApJ* , 574, 740
Utsumi Y., Goto T., Kashikawa N., et al., 2010, *ApJ* , 721, 1680
Wang R., Carilli C. L., Neri R., et al., 2010, *ApJ* , 714, 699
Weidinger M., Møller P., Fynbo J. P. U., Thomsen B., 2005, *AAp* , 436, 825
Willott C. J., Albert L., Arzoumanian D., et al., 2010, *AJ* , 140, 546
Willott C. J., Chet S., Bergeron J., Hutchings J. B., 2011, arXiv:1109.4110
Willott C. J., Delorme P., Omont A., et al., 2007, *AJ* , 134, 2435
Yu Q., Lu Y., 2005, *ApJ* , 620, 31